Available online at www.sciencedirect.com
SCIENCE DIRECT
Journal of Sound and Vibration 297 (2006) 391–407
JOURNAL OF SOUND AND VIBRATION
www.elsevier.com/locate/jsvi

A characterization of frequency–temperature–prestress effects in viscoelastic films

Gérald Kergourlay*, Etienne Balmès, Gilbert Legal

MSSMat, Ecole Centrale Paris, 92295 Chatenay Malabry Cedex, France

Received 6 September 2004; received in revised form 10 April 2006; accepted 10 April 2006
Available online 30 June 2006

Abstract

Viscoelastic materials can be used to design efficient damping treatments. The design of well-damped structures typically requires significant numerical optimizations which rely on proper material characteristics. The present study was motivated by applications where an initially flat viscoelastic sandwich is press formed. Constitutive laws, that gave good correlation for the flat plate, led to poor correlation in bent configurations. It is well known that the properties significantly depend on frequency, temperature but also on other environmental factors such as static prestress. None of the classical techniques being suited to the determination of static prestress effects, a new test rig allowing dynamic measurement of complex shear modulus of a thin film under significant static loading was thus needed. The design and experimental validation of this rig are presented, and some results on the characterization of frequency–temperature–prestress effects in a sandwich plate and their representation using the superposition hypothesis are discussed.

1. Introduction

The use of constrained layer viscoelastic treatments is a well-established procedure to enhance damping in structures [1–3]. The transmission of dynamic shear loads through the viscoelastic material generates energy dissipation in the form of heat. The design of well-damped structures typically requires significant numerical optimizations [4,5] which rely on proper material characteristics.

The present study was motivated by applications, where an initially flat viscoelastic sandwich [6] is press formed. Constitutive laws, that gave good correlation for the flat plate, led to poor correlation in bent configurations. It is well known that the properties significantly depend on frequency, temperature and other environmental factors such as static prestress.

The damping properties can be determined experimentally using direct and indirect techniques. These tests are based on approaches which are relevant on different frequency ranges:

- classical beam tests (indirect measurements producing modal damping ratio) [7];
- dynamic shear and torsional rheology (10^{-5}–10^{2} Hz) [8];
- ultrasonic spectrometer (up to several MHz) [9].

*Corresponding author. Tel.: +33 1 44 24 64 12; fax: +33 1 44 24 64 11.
E-mail addresses: gerald.kergourlay@paris.ensam.fr (G. Kergourlay), balmes@ecp.fr (E. Balmès), legal@ecp.fr (G. Legal).

0022-460X/$ - see front matter © 2006 Elsevier Ltd. All rights reserved.
doi:10.1016/j.jsv.2006.04.003

The most common indirect measurements use modal damping ratios of classical composite beam systems (homogeneous, Oberst [7], modified Oberst, sandwich tests). By studying the various resonances of the damped beam, the effect of frequency on the properties of the material can be established.

A significant number of measurement points can be examined by changing the beam dimension and temperature. A seminal contribution to the analysis of damping films through the shear tests of three-layer beams has been realized as early as in 1959 by Ross, Ungar and Kerwin (RUK) [10]. The analytical formulation RUK relates the modal damping ratio and the complex modulus properties.

Direct techniques correspond to excitation in extension, torsion or shear of polymer samples where the dynamic response is obtained at all excitation frequencies, leading directly to the complex modulus. These are known as *direct complex stiffness* (DCS) test systems [11] and this is the approach retained here.

Since none of the classical techniques is suited to the determination of static prestress effects on a wide physical frequency range starting at low frequencies, a new test rig allowing dynamic measurement of complex shear modulus of a thin film under significant static loading was needed to understand the source of the difficulties with bent plates. The present study discusses the design and experimental validation of this rig, and some results on the characterization of a particular material.

Section 2 details the dynamic rig to measure directly the complex shear stiffness of viscoelastic films, its functional principle, dimensioning and experimental realization. The rig is effective over a relatively narrow frequency band, but by performing measurements at different temperatures and using the frequency–temperature superposition hypothesis [2], the frequency domain can be extended to a wide range. It is also proposed to use the superposition hypothesis to represent prestrain effects, investigating the validity of this approach in a substantially sheared material. Section 3 deals with the experimental data processing and the construction of viscoelastic tabulated laws in the frequency range 1–2000 Hz, for temperatures of 0–50 °C and what is new, for prestrain up to 3 applied to a viscoelastic sandwich plate with polymer form core provided by Arcelor [6].

2. Test rig design and validation

Section 2.1 presents the rig and the test facility. Section 2.2 details the simplified modeling as a two mass system connected by a viscoelastic spring (shear layer) in parallel with an elastic spring representing the prestress beam. This functional model will be used to treat the experimental data. Section 2.3 presents the finite element (FE) model used to design the geometry of the rig in order to isolate the shear mode from other perturbing modes on the widest frequency band. Section 2.4 finally deals with the evaluation of the frequency/storage modulus/loss factor range where the mechanical properties of damping sandwich plates are predicted with a weak error ratio.

2.1. Rig construction

One aims at measuring the material properties of the viscoelastic core of a steel/polymer/steel sandwich plate through a direct solicitation in shear. The tested sandwich plates have been kindly provided by Arcelor [6] and are labeled BI2F through this study. This sandwich plate model is available under the commercial denomination Usiconfort in the automotive industry and Sollight AC in the building industry. The BI2F sample is made of a 0.04 mm polymer viscoelastic core and two 0.5 mm steel layers. To obtain an uniform shear stress-state in the viscoelastic polymer core of the steel–polymer–steel sandwich plate, the steel stiff layers are selectively cut in order to isolate a test zone in the viscoelastic core: the top layer is designed to translate, whereas the bottom layer will be clamped (Fig. 1).

The test rig is made up with additional structural elements (moving part, static frame) shown in Fig. 2, and realized in standard steel for its high rigidity and milling ability. The milled steel–polymer–steel sandwich plate is glued and screwed to the static frame. The moving part consists of two elements fixed to the sandwich top layer and of an aperture so that a transverse beam can stiffen the connecting of the bottom layer to the static frame.

To induce prestrain in the viscoelastic test zone, a prestress beam whose position is adjusted by set screws has to be added to the rig (Fig. 2). A Hall effect position sensor Kaman KD 2300 is set on a flask at the back of the rig in order to measure the static displacement induced by the prestress beam and the dynamic relative displacement of the moving part. A force sensor Brüel–Kjaer BK 8200 measures the dynamic force induced by

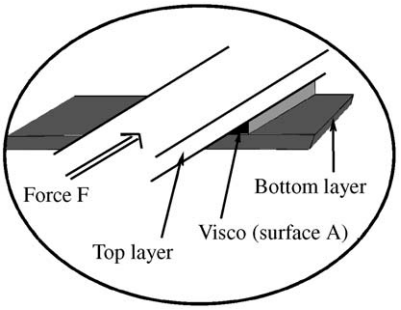

Fig. 1. Milled steel/polymer/steel sandwich plate layers—viscoelastic test zone.

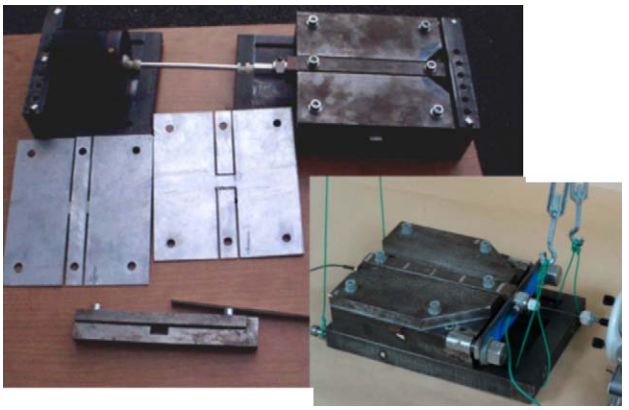

Fig. 2. Complete test rig+milled viscoelastic plates and moving part (left); prestress beam mounted on the test rig front (right).

an electrodynamic shaker LDS V101 through a piano-wire at the moving part entry and the whole rig is hung at his corners. To study the influence of the temperature on the material properties, the test rig is put in an isothermal chamber with temperature control.

In the assumption of a perfect rigidity of the moving part and of the rig other elements in the measuring frequency range (Section 2.3 discusses the importance of this assumption), these measures exactly correspond to the shear of the viscoelastic test zone. All measurements are done using LMS measuring system CadaX, Scadas II [12], connected to a HP workstation and their analysis is proceeded under Matlab/SDT [13].

Each measurement is performed with a random excitation between 0 and 2048 Hz. One obtains the relative displacement to force frequency response function (FRF) shown in Fig. 3 for two excitation force levels at a temperature of 23 °C in presence of the prestress beam but with no prestrain. The comparable FRF shapes means that there is a very good nonlinearity level of the measure. A good reproducibility has been also achieved. One can mainly observe the shear mode resonance around 1000 Hz, but also other perturbing modes: perturbations at low frequencies which correspond to suspension modes and a mode at 1400 Hz that will be explained in Section 2.3.

2.2. Functional principle

This section details the simplified analytical model used to determine the complex modulus from actual measured FRF.

For a test zone of surface A and a dynamic shear force F_s induced in the top layer, the shear stress σ_{13} in the viscoelastic core is equal to F_s/A. The associated strain ε_{13} can be approximated by

$$\varepsilon_{13} = \frac{1}{2}\left(\frac{\partial u_1}{\partial x_3} + \frac{\partial u_3}{\partial x_1}\right) \simeq \frac{1}{2}\frac{\partial u_1}{\partial x_3} \simeq \frac{1}{2}\frac{d_r}{h}, \tag{1}$$

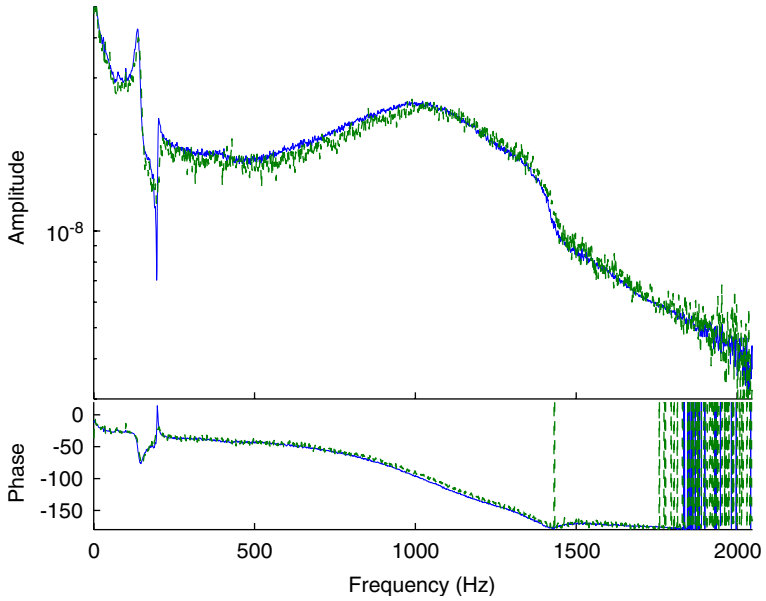

Fig. 3. Experimental relative displacement to force FRF on 1–2048 Hz at 23 °C for two force levels: — F, −− $F/4$. With prestress beam.

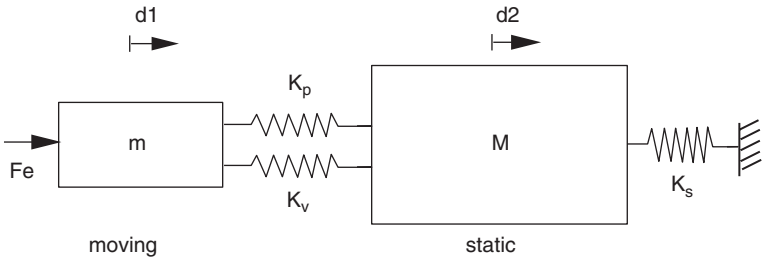

Fig. 4. Functional model.

since one assumes that there is no thickness variation of the viscoelastic core (i.e. $\partial u_3/\partial x_1 \simeq 0$), the viscoelastic test zone being indeed thin compared with its other dimensions. d_r and h, respectively, stand for the shear displacement (induced by force F_s) and the thickness of the viscoelastic test zone. The complex shear modulus G^* is thus given by

$$G^*(\omega, T, \varepsilon_0) = \frac{1}{2}\frac{\sigma_{13}}{\varepsilon_{13}} = \frac{h}{A}\frac{F_s(\omega)}{d_r(\omega, T, \varepsilon_0)}, \tag{2}$$

which is proportional to the force to displacement FRF F_s/d_r, at frequency ω, temperature T and prestrain $\varepsilon_0 = d_0/h$, where d_0 stands for the static shear displacement. The F_s/d_r FRF is however not directly accessible, so that it will be obtained using a functional representation of the rig.

One considers the functional model shown in Fig. 4. m stands for the moving part mass fixed to the test zone top layer and M for the static frame mass to which the bottom layer is clamped; K_p represents the stiffness of the prestress beam, K_s the rig suspension stiffness; the complex frequency–temperature–prestrain dependent stiffness $K_v(\omega, T, \varepsilon_0) = G^*(\omega, T, \varepsilon_0)A/h$ models the viscoelastic test zone. The corresponding matrix system can be written as

$$\left((K_p + K_v)\begin{bmatrix} 1 & -1 \\ -1 & 1 \end{bmatrix} + \begin{bmatrix} 0 & 0 \\ 0 & K_s \end{bmatrix}\right)\begin{Bmatrix} d_1 \\ d_2 \end{Bmatrix} - \begin{bmatrix} m & 0 \\ 0 & M \end{bmatrix}\begin{Bmatrix} d_1 \\ d_2 \end{Bmatrix}\omega^2 = \begin{bmatrix} F_e \\ 0 \end{bmatrix}. \tag{3}$$

Assuming K_s to be small, and given measurements of external force F_e and relative displacement $d_1 - d_2$, a straightforward manipulation of Eq. (3) leads to

$$\frac{F_s(\omega)}{d_1(\omega) - d_2(\omega)} + K_p = K_v(\omega, T, \varepsilon_0) + K_p = G^*(\omega, T, \varepsilon_0)\,\frac{A}{h} + K_p$$
$$= \frac{M}{M+m}\left(\frac{F_e(\omega)}{d_1(\omega) - d_2(\omega)} + m\omega^2\right). \quad (4)$$

This expression will be used to predict G^* from experimental FRF measurements over the widest possible frequency range for various temperatures and prestrains.

2.3. Design of test rig using FE modeling

As explained in the previous section, the test rig principle is based on an unique shear mode operation but in reality there are other perturbing modes already illustrated by Fig. 3. A FE model will predict the dynamic behavior, and help to design the test rig geometry so as to obtain the widest frequency range with no mode excited other than the shear mode.

Fig. 5 presents the FE model of the test rig: 7024 solid elements are used for the static frame, moving part, support, flask, glue, layers and viscoelastic core; 116 beam elements for the screws, excitation stinger and prestress beam; 1 mass element for the shaker. The different material properties are summarized in Table 1.

A nominal elastic modulus $E_0 = 50\,\text{MPa}$ has been chosen for the viscoelastic core. Fig. 6 shows four selected mode shapes of the model hung up at its corner with four springs of stiffness $K_0 = 10^6\,\text{N/m}$.

The functional test rig mode (shear mode) occurs at 1877 Hz (mode 14). Other modes correspond to rocking of the moving part around the viscoelastic test zone in directions (Oz) and (Ox) (modes 8 and 10) and to its first bending mode (mode 12). These three modes will perturb the FRF evaluation since they also stress the viscoelastic test zone. The rocking modes are relatively low frequency and should thus not perturb measurements too much. The bending mode is more critical. The rig can only be used if the shear mode resonance is well separated from the bending mode.

We can now test the assumption of a rigid moving part during the shear mode (mode 14). Table 2 presents the resonant frequency variations of the modes when changing the viscoelastic film stiffness: the higher the stiffness, the higher the frequencies. The last line shows the evaluation of the shear resonant frequency using the equivalent model of Eq. (3): there is a growing difference between the functional and the FE shear frequency evaluations when increasing the film stiffness. This is explained by the growing flexibility of the

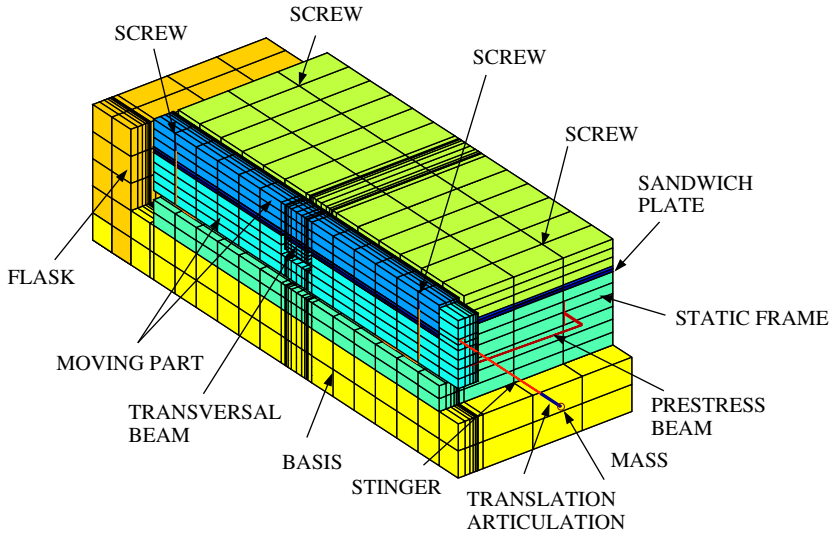

Fig. 5. Test rig FE model, half-section.

Table 1
Test rig mechanical properties

Steel	$E = 210\,\text{GPa}$	$v = 0.29$	$\rho = 7800\,\text{kg/m}^3$
Glue	$E = 1\,\text{GPa}$	$v = 0.49$	$\rho = 1100\,\text{kg/m}^3$
Polymer (core)	$E_0 = 50\,\text{MPa}$	$v = 0.49$	$\rho = 1200\,\text{kg/m}^3$
Screw	$\phi = 7\,\text{mm}$	Steel	
Prestress beam	$A = 2\,\text{mm} \times 26\,\text{mm}$	Steel	
Shaker stinger	$\phi = 1\,\text{mm}$	Steel	
Shaker	$m = 0.6\,\text{kg}$		

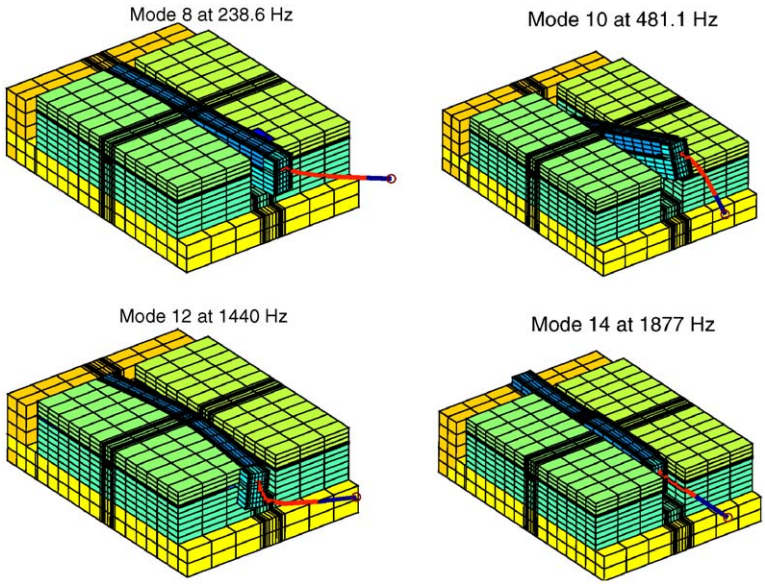

Fig. 6. Normal modes for $\text{Re}(G^*)/G_0 = 1$ (without prestress beam).

Table 2
Resonance frequencies—f_0 in Hz vs. the value of $\text{Re}(G^*)/G_0$

$\text{Re}(G^*)/G_0$	0.02	0.05	0.2	1	2
Rocking mode (Oz)	35	55	110	239	328
Rocking mode (Ox)	144	215	350	481	518
Bending mode	287	445	832	1441	1644
Shear mode (Oy)	292	459	902	1877	2479
Functional model	292	461	923	2063	2918

moving part: the higher the shear modulus, the greater the deformation of the moving part, so that the predicted resonant frequency is weaker compared to the functional model.

Since the aim is to produce prestrain in the viscoelastic core, it is also necessary to study the influence of adding a prestress beam to the FE model. The bending mode (mode 12 of Fig. 6) is moved to a higher frequency outside the band of interest so that it no longer perturbs the results significantly. But the prestress beam presence increases the (Ox) rocking mode frequency from 416 to 1481 Hz and this mode will perturb the prestrain measurements since it is in the frequency range of interest. Fig. 7 shows a comparison of the (Ox) rocking and shear modes for the FE models with (left) and without (right) prestress beam. The prestress beam has a very slight influence on the shear mode frequency, increasing it by only 5 Hz.

The displacement to force FRFs have been evaluated over the frequency range 0–2048 Hz for the prestress beam configuration using a real viscoelastic constitutive law at various temperatures. A reduced computation with error control [14] enables to compute many frequencies and temperatures with a reasonable computing time. Fig. 8 shows how changes occur to the shear resonant frequency and FRF phase when varying temperature; the (Ox) rocking mode around 1400 Hz appears to have a large influence at every temperature. Comparison of the corresponding experimental FRF measured at 23 °C (Fig. 3) with the FE FRF allows to understand that the perturbing mode at 1400 Hz corresponds to the predicted (Ox) rocking mode of Fig. 7 (mode 13).

2.4. Detailed analysis

The following paragraphs deal with the evaluation of the frequency/storage modulus/loss factor range for which the mechanical properties of damping sandwich plates (with the same geometrical characteristics as the BI2F plate) can be measured with small relative errors (less than 15%).

The validity of the stress–strain uniformity assumption has first to be studied. To do so, a static computation is performed on the complete rig with a detailed mesh of the test zone. Fig. 9 shows the strain

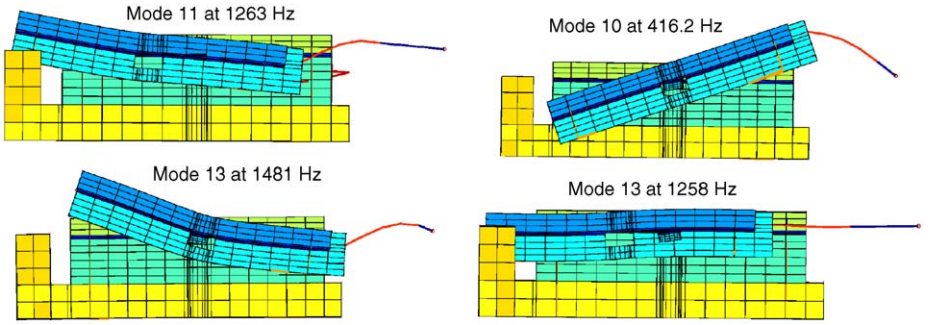

Fig. 7. Normal modes with (left) and without (right) prestress beam, half-section.

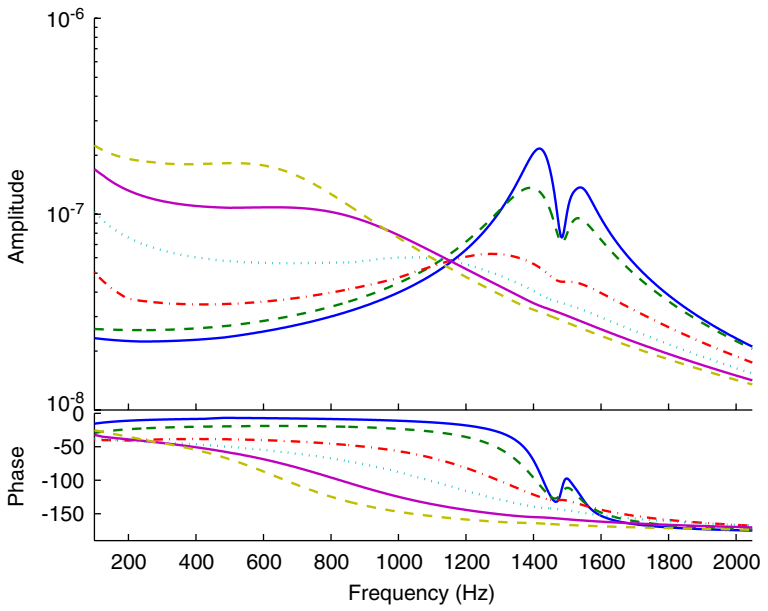

Fig. 8. FE displacement to force FRF 100–2048 Hz with prestress beam at various temperatures: — 0 °C, –– 10 °C, · – · · 20 °C, · · · 30 °C, — 40 °C, –– 50 °C.

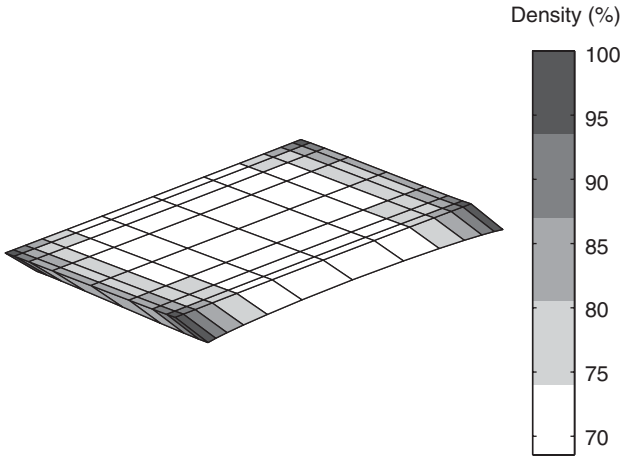

Fig. 9. Strain energy density repartition in the viscoelastic test zone.

energy density in the test zone. A non-uniform repartition of strain energy can be observed, the differences being mainly located at the boundaries where the variation is up to 30%. But the more detailed the test zone mesh, the wider the stress–strain uniformity and the bigger the variation: these are border effects as explained in Ref. [15]. One can thus assume the validity of the stress–strain uniformity assumption and apply Eq. (4) to the FRFs in order to get the complex shear modulus G^*.

One calls the real part $G'(\omega) = \mathrm{Re}(G^*(\omega))$ the *storage modulus*; the *loss factor* is the ratio of imaginary part to the real part, $\eta(\omega) = \mathrm{Im}(G^*(\omega))/\mathrm{Re}(G^*(\omega)) = G''/G'$. By applying Eq. (4) to the model, one gets the frequency/storage modulus/loss factor range where the properties are well evaluated. The estimated storage modulus $\mathrm{Re}(G_e)$ and loss factor η_e are compared to the nominal values G' and η initially put in the FE model. Their variation is illustrated by an error expressed in percentage form: $100 * [\mathrm{Re}(G_e)/\mathrm{Re}(G^*) - 1]$ for the storage modulus and $100 * [\eta_e/\eta - 1]$ for the loss factor. This variation comes from the fact that the FE computation takes into account stiffness of the other parts of the test rig. This measurement validity domain can be interpreted as an error map which may be used to slightly improve the experimental identification of G' and η.

Fig. 10 shows the estimated storage modulus for various nominal moduli $G' \in [10^5\text{–}10^8]$ Pa for $\eta = 0.01$ (left) and $\eta = 0.7$ (right). The storage moduli are underestimated, with an error that increases as the real part of G' is increased, or as the frequency decreases. The error does not go beyond -15% over 580–1412 Hz.

A similar analysis for various loss factors $\eta \in [0 - 1]$ is illustrated in Fig. 11 for two nominal moduli $G = G_0$ (left) and $G = G_0/10$ (right). The error does not pass -7% over 580–1412 Hz and hardly depends on η.

3. Experimental data processing

3.1. Complex modulus measurements

Figs. 12 and 13 present the displacement to force FRFs at various temperatures 0, 5, 10, 15, 17, 23, 25, 35, 50 °C without prestress beam, and for prestrains $0, 0.62, 1.36, 1.57, 1.76, 2.34$ at a temperature of 23 °C. These FRFs have been smoothed using a sliding average.

One can directly estimate the complex shear modulus G^* from the measurements of relative displacement to force FRFs using Eq. (4). To do this, one needs to know the experimental values of K_p, M and m. Weighing provides the value of $(M + m)$. Transforming the relative displacement to force FRF to its equivalent acceleration to force FRF supplies the inverse of m: its high frequency asymptote corresponds to the inertia of the moving part mass m. As for K_p, the same FRF is measured on the rig with a milled sandwich plate with no viscoelastic core. The real stiffness of the prestress beam K_p is then directly measured at $\omega = 0$ using Eq. (4), since $K_v = 0$ and $M/(M + m)$ is known.

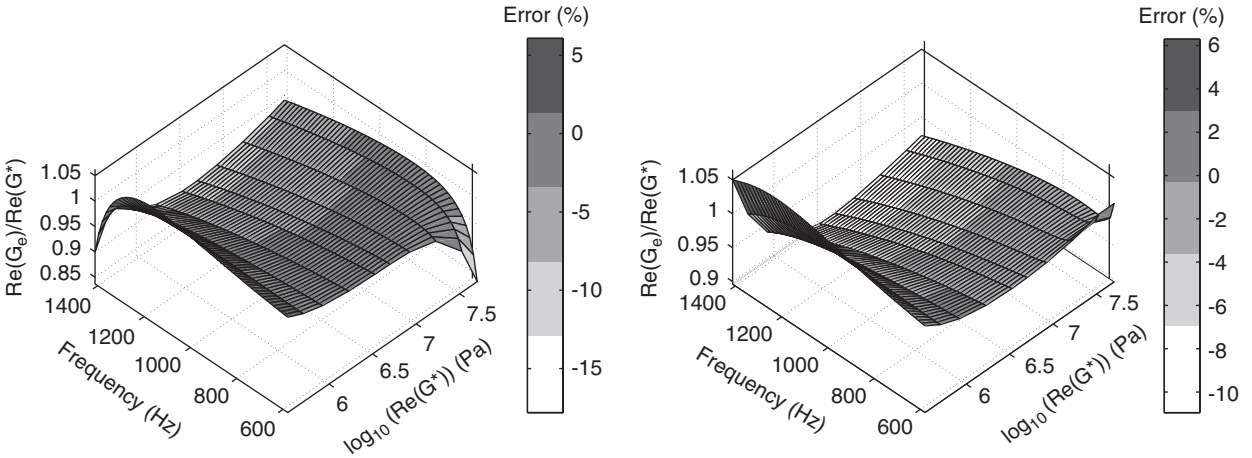

Fig. 10. Estimated storage modulus $\mathrm{Re}(G_e)$ for various $G*$ with $\eta = 0.01$ (left) and $\eta = 0.7$ (right); 580–1412 Hz. Without prestress beam.

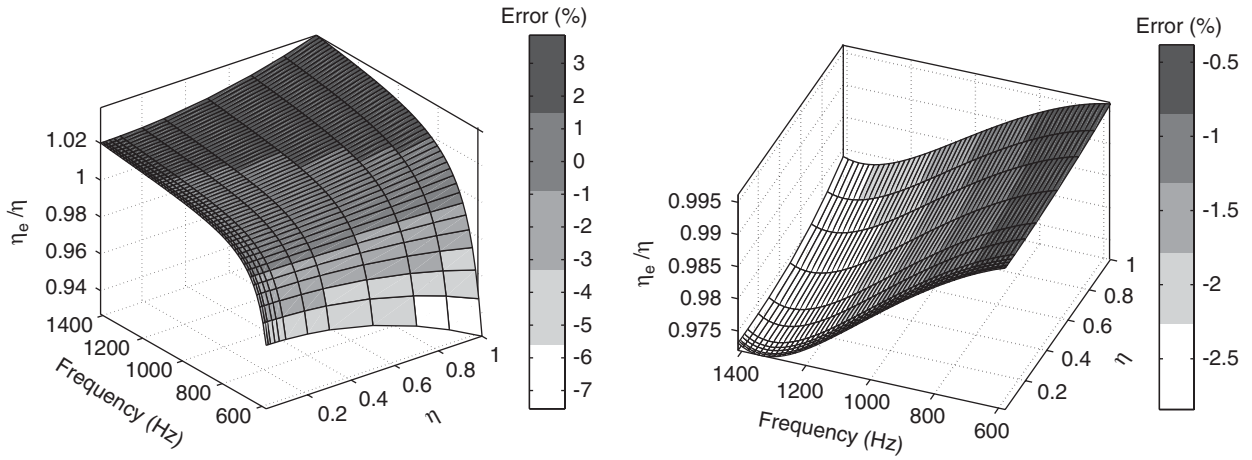

Fig. 11. Estimated loss factor η_e for various $\eta = G''/G'$ with $G = G_0$ (left) and $G = G_0/10$ (right); 580–1412 Hz. Without prestress beam.

Eq. (4) is then applied to the two FRFs to get G' and η as represented in Figs. 14 and 15. One can see the strong variation of both G' and η over the range 0–2048 Hz for temperatures of 0–50 °C and prestrains up to 2.34 (3 is the prestrain limit before delamination of the core).

3.2. Principles of reduced frequency representations

The basic assumption of linear viscoelasticity [16] is the existence of a relaxation function such that the stress $\sigma(t)$ is obtained as a convolution with the strain history $\varepsilon(t)$. Using the Fourier transform, one obtains an equivalent representation where the material is now characterized by the *Complex Modulus* Λ (transform of the relaxation function).

For all practical purposes, one can thus, in the frequency domain, deal with viscoelasticity as a special case of elasticity where the material properties are complex. In practice, it is very difficult to generate combined dynamic loads so that one only tests one particular component of the viscoelastic tensor Λ. Compression tests give the complex Young's modulus E^* and shear tests the complex shear modulus G^*.

It is however easily tested that the complex modulus depends significantly on environmental factors (temperature, prestrain, etc.). Measurements of complex stiffness over a fixed frequency band are made at various temperatures in the transition region. It has been experimentally observed that a continuous curve for

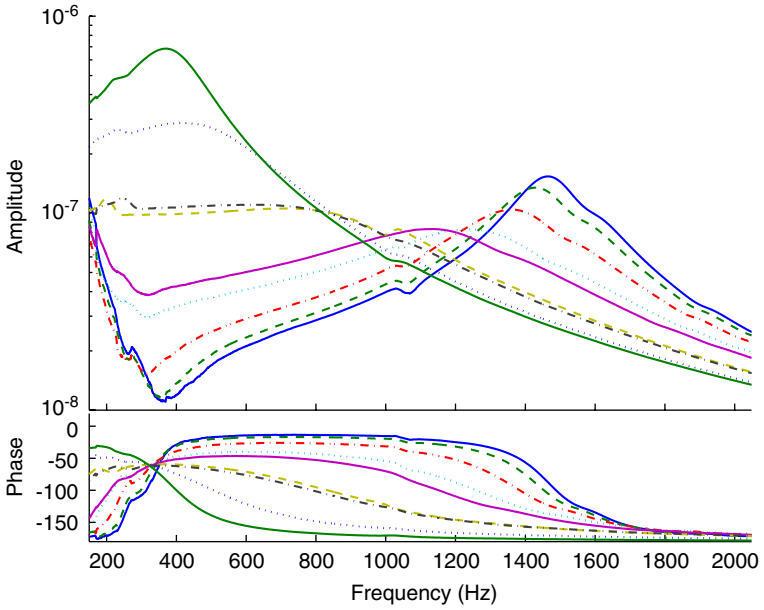

Fig. 12. Displacement to force FRF 150–2048 Hz at various temperatures: — 0 °C, −− 5 °C, · − ·· 10 °C, · · · 15 °C, — 17 °C, −− 23 °C, · − ·· 25 °C, · · · 35 °C, — 50 °C.

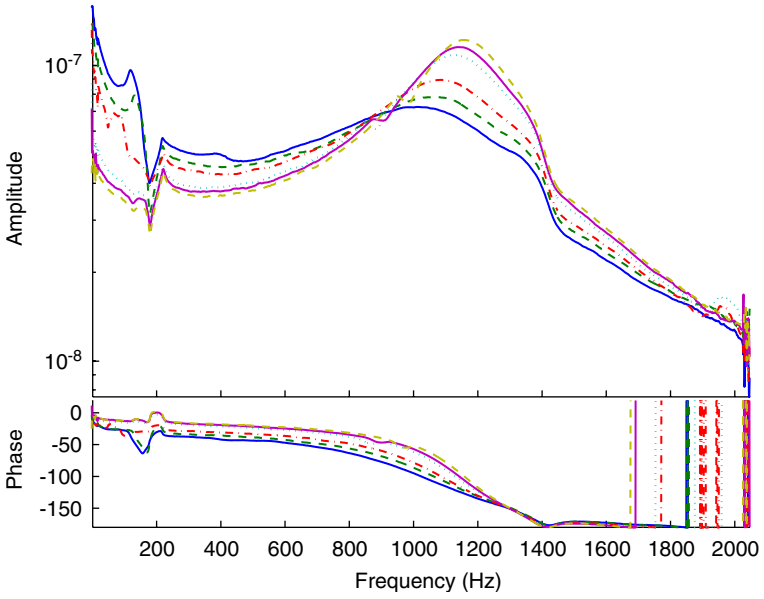

Fig. 13. Displacement to force FRF 1–2048 Hz at various prestrains: — 0, −− 0.62, · − ·· 1.36, · · · 1.57, — 1.76, −− 2.34. $T = 23\,^{\circ}\mathrm{C}$.

the storage modulus G' and loss factor η can be obtained by translating, with respect to frequency, moduli obtained at different temperatures. In other words, G^* is a function of $\omega\alpha(T)$ (where $\alpha(T)$ is called a shift function) rather than ω and T separately. This property is called the *frequency–temperature superposition hypothesis* [2]. The continuous G' and η functions are called *master curves*. The product $\omega\alpha(T)$ is called the *temperature-reduced frequency*.

These translations are completely defined by the values of the temperature shift function $\alpha_T = \alpha(T)$ at the different measured temperatures T. Possible parametric representations, based on the physical dissipation processes, are discussed in Ref. [17] and can be directly tested on the measured data obtained at various

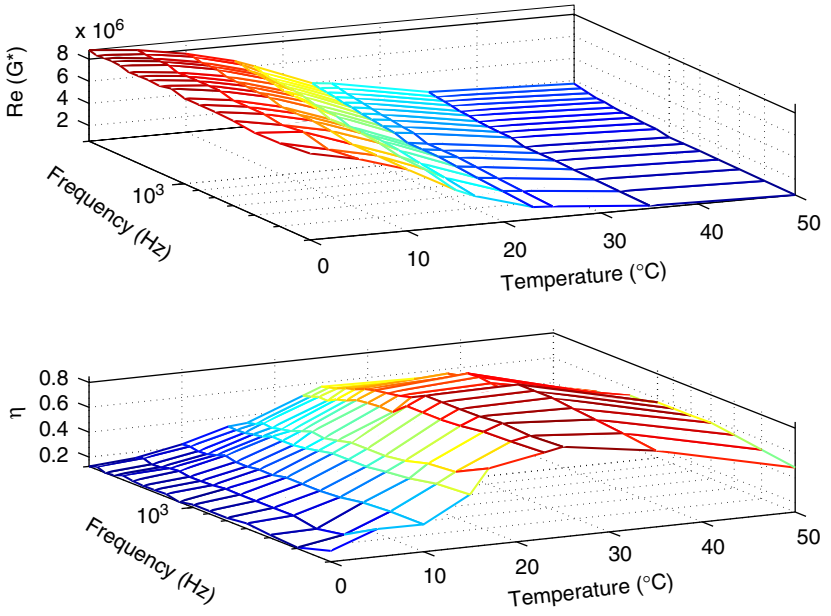

Fig. 14. BI2F complex shear modulus, 400–2000 Hz. $T \in 0$–$50\,^{\circ}\mathrm{C}$, $\varepsilon_0 = 0$.

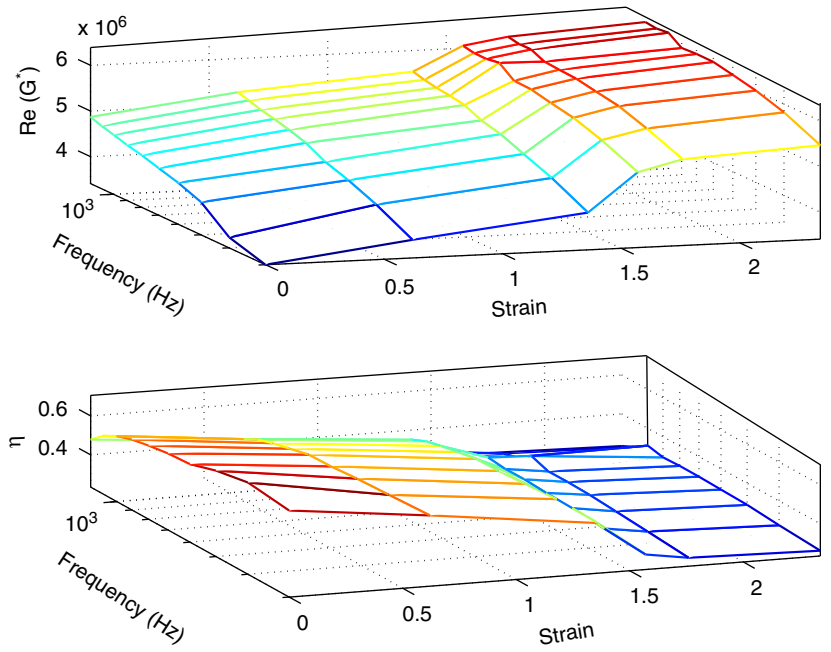

Fig. 15. BI2F complex shear modulus 150–1700 Hz.$\varepsilon_0 \in 0$–2.34, $T = 0\,^{\circ}\mathrm{C}$.

temperatures to obtain a single curve over the reduced frequency range. A simple, thermally activated process will follow an Arrhenius behavior and will adequately describe α_T up to the transition temperature (where the peak of the loss factor occurs):

$$\log \alpha_T = \frac{E_a}{R}\left(\frac{1}{T} - \frac{1}{T_0}\right), \tag{5}$$

where $R = 8.314 \times 10^{-3}\,\mathrm{kJmol^{-1}\,K^{-1}}$, E_a is the mean activation energy and T_0 the reference temperature.

The Williams–Landel–Ferry (WLF) [18] equation is appropriate beyond the transition temperature:

$$\log \alpha_T = -\frac{C_1^0(T - T_0)}{C_2^0 + T - T_0}. \tag{6}$$

The viscoelastic coefficients C_1^0 and C_2^0 depend on the material, and their values are functions of the reference temperature T_0.

In Section 3.3 we will verify that the superposition hypothesis is indeed an useful technique to extend the frequency range of validity to various temperatures. The extension of this hypothesis to prestrain effects will be addressed in Section 3.4.

3.3. Validation for temperature effects

The ability to build master curves from temperature/frequency maps of Fig. 14 is discussed here. One manually translates, in frequency, the 400–2000 Hz isothermal curves in order to obtain one single sigmoidal continuous curve for G' in the temperature-reduced frequency range (Fig. 16 left). The same manual shift function is applied to the loss factor η (Fig. 16 right). One observes that it defines a convex shaped curve and a rather good superposition of the low temperature (below 23 °C) segments. Beyond 23 °C, at temperatures 25, 35 and 50 °C, the master curve is however not perfectly continuous: the curves are not strictly tangent when they overlap. The applicability of the temperature superposition hypothesis to measurements over the whole temperature range is discussed below.

Fig. 17 shows the resulting temperature shift factors with their variation zone delimited by the minimum and maximum values. The measured values are compared with two formulations of the WLF equations (6). These formulations are defined with the classical values $C_1^0 = 17.4$ and $C_2^0 = 51.6$ °C proposed in Ref. [18], and also for C_1^0 and C_2^0 values identified from the chosen manual shift factors. Differences exist but the global shape is in agreement with the analytic formulation. As concerns the minimum and maximum values, they have been obtained by modifying the reference physical frequency range according to two cases. Using the same frequency response function measurements (that have been shown to be reproducible in Section 2.1), it was decided to change the initial physical frequency range 400–2000 to 450–925 Hz and then to 1500–1970 Hz, in order to avoid the 1400 Hz (Ox) rocking mode. This resonance is clearly visible in Fig. 16: the curves present a peak at low temperatures and changes in the tangency slope at high temperatures for both the storage modulus and the loss factor. It appears that the manual shift factors needed to obtain good continuity of the master curve vary significantly, particularly at temperatures at temperatures 23–25, 35 and 50 °C. This is in

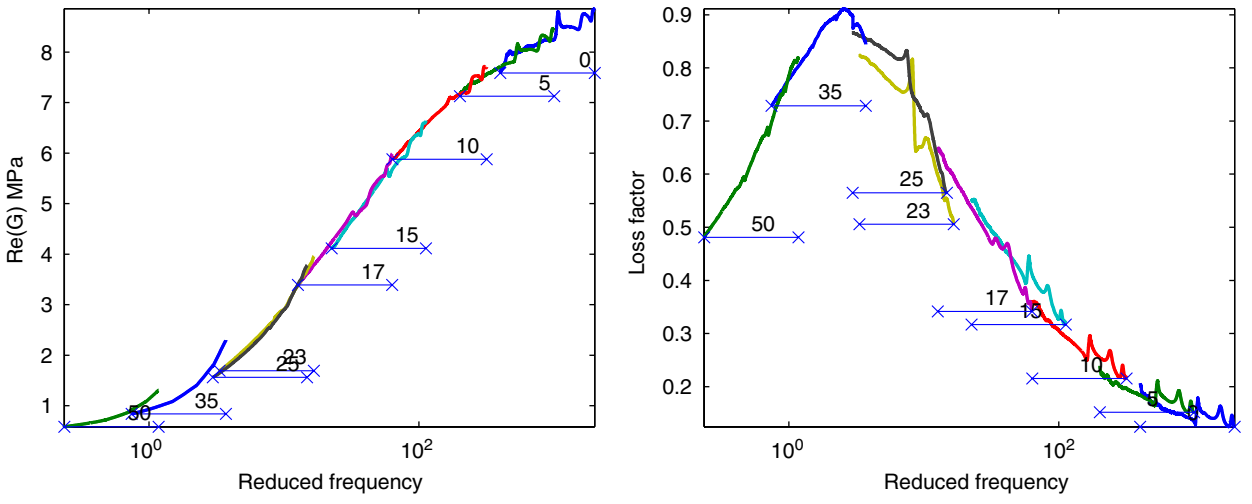

Fig. 16. Storage modulus (left) and loss factor (right) against temperature-reduced frequency $\omega\alpha_T$. $T \in [0, 5, 10, 15, 17, 23, 25, 35, 50]$°C, $\varepsilon_0 = 0$.

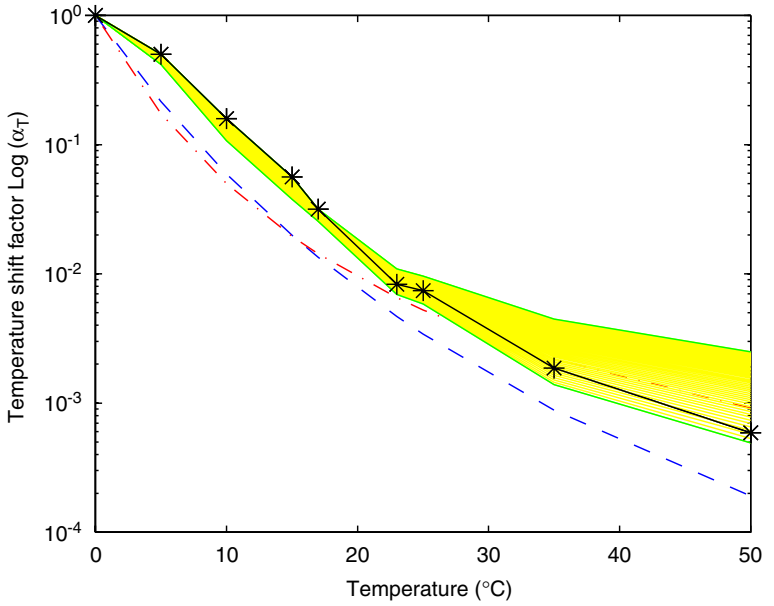

Fig. 17. Temperature shift factor α_T against temperature T for BI2F. $-*$ Manual shift + variation zone of manual shifts, and two typical WLF equations: – $-17.4\Delta T/(51.6+\Delta T)$, · – · $-10.5\Delta T/(25+\Delta T)$. $T \in 0$–$50\,^{\circ}$C.

accordance with the observation already made in Fig. 16: the superposition hypothesis can be criticized at those temperatures that correspond to the loss peak for the BI2F sample. The fact that uncertainty exists concerning the choice of the manual shift factors could have been overcome by reducing the temperature interval to provide more data in this region. Unfortunately, not many points could be measured at high (as well as at low) temperatures since it was difficult to ensure a constant temperature in the isothermal chamber during the measurements. Keeping in mind the uncertainty that exists concerning the loss peak region, it was finally considered quiet reasonable to apply the frequency–temperature superposition hypothesis to these measurements.

Finally, the measurements are smoothed and undersampled to produce a table against reduced frequency. This has been applied to the experimental master curve in temperature-reduced frequency: Fig. 18 is the undersampled tabulated law of Fig. 16. These tables, with proper extrapolation procedures, can be used to predict the complex shear modulus at arbitrary frequencies and temperatures (as shown in Fig. 18) for FE analysis of models containing this material.

For this material, cross validations have been performed by predicting the response of a square sandwich plate at various temperatures. Comparison of experimental acceleration upon force FRFs to predictions using the reduced-temperature tabulated constitutive law of BI2F shows very good results [19]. It shows the applicability of the superposition hypothesis to temperature effects and the use of tabulated laws in the FE analysis.

3.4. Applicability to prestrain effects

To test the applicability of the superposition hypothesis to frequency–prestrain effects, the same procedure is applied to the measurements at various prestrains: Fig. 19 (obtained from the prestrain/frequency map of Fig. 15) and Fig. 20 present the results at two temperatures 23 and $35\,^{\circ}$C. Following the definition of the temperature-reduced frequency introduced in Section 3.2, a reduced frequency called the prestrain-reduced frequency has been defined as

$$\omega\alpha(\varepsilon_0) = \omega\alpha_{\varepsilon_0}, \tag{7}$$

where α_{ε_0} is the prestrain shift factor.

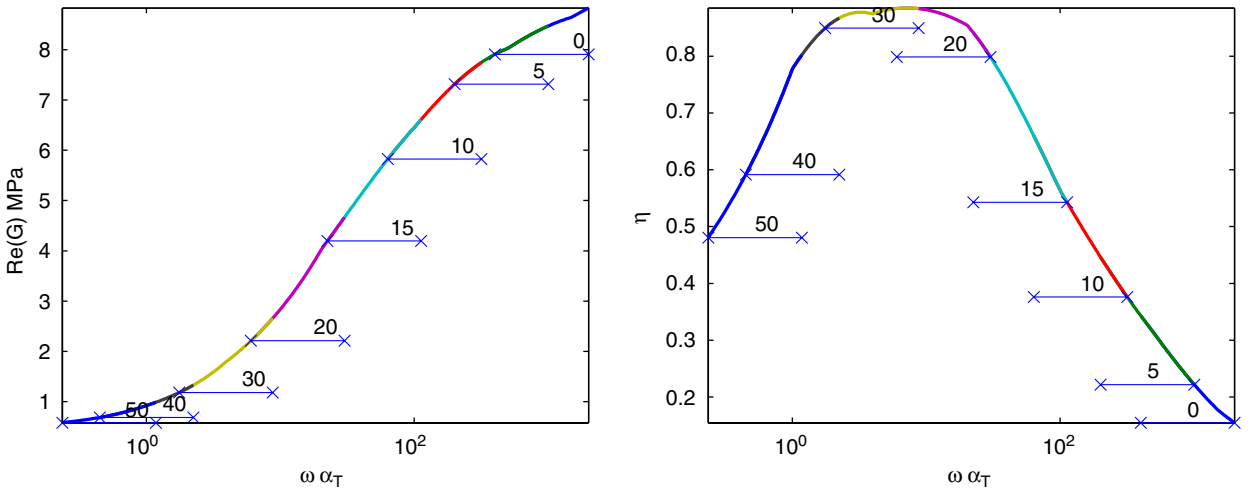

Fig. 18. Undersampled master curve against temperature-reduced frequency $\omega\alpha_T$. $T \in [0, 5, 10, 20, 30, 40, 50]^\circ$C.

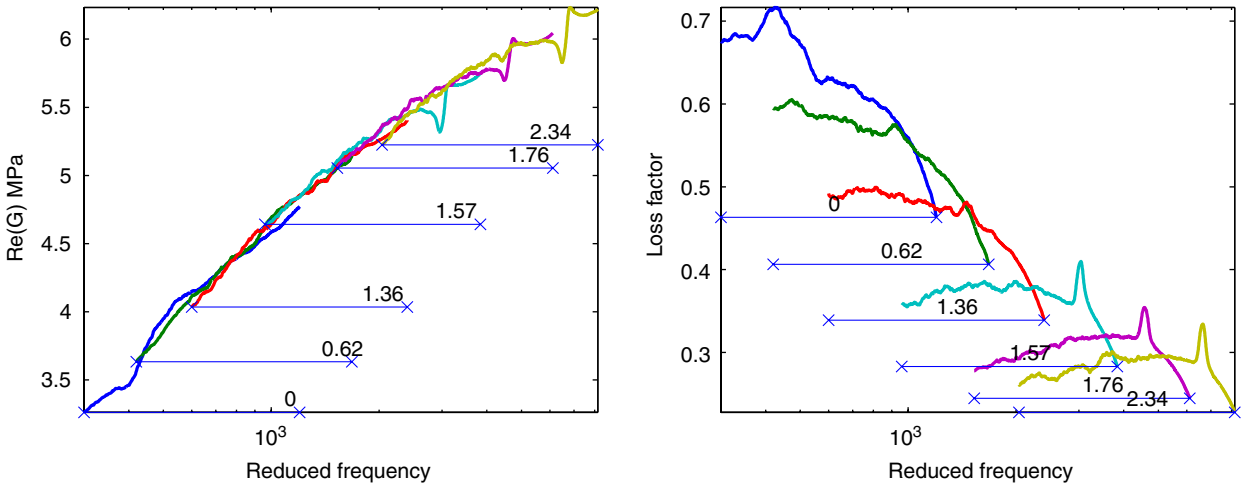

Fig. 19. Storage modulus (left) and loss factor (right) against prestrain-reduced frequency $\omega\alpha_{\varepsilon_0}$ (cf. Eq. (7)). $\varepsilon_0 \in [0, 0.62, 1.36, 1.57, 1.76, 2.24]$, $T = 23\,^\circ$C.

A manual prestrain shift factor has been applied to the 150–1700 Hz prestrained curves of G' in order to obtain one continuous curve in the prestrain-reduced frequency range. The same manual shift function is applied to the loss factor η (Fig. 16 right). One observes that it globally defines an increasing curve for the modulus (by nearly a factor of 2) and a decreasing curve for the loss factor. This is the expected behavior described by many authors. But the tangency of the curves when they overlap is not realized.

The low and high parts of each data do not superimpose and a peak is visible, particularly in the loss factor estimation of each prestrained curve. The modal resonance associated to this peak is quite visible in Figs. 3 and 13 and was seen to be the (Ox) rocking mode according to the FE analysis. The greater the prestrain, the greater the degree of misfit in the master curve: the (Ox) rocking mode is more and more visible and the tangency of the curves where they overlap more and more different. This is particularly observable at temperature 23 °C for the loss factor (Fig. 19). At temperature 35 °C (Fig. 20), the loss factors of each prestrain segment are clearly not tangent with one another but the fact that the

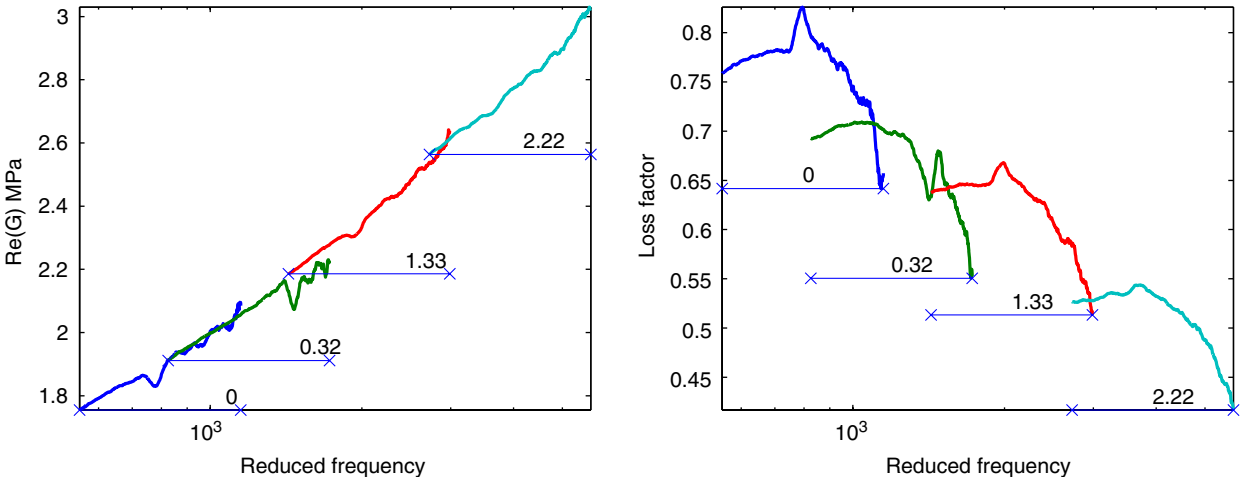

Fig. 20. Storage modulus (left) and loss factor (right) against prestrain-reduced frequency $\omega\alpha_{\varepsilon_0}$ (cf. Eq. (7)). $\varepsilon_0 \in [0, 0.32, 1.33, 2.22]$, $T = 35\,^{\circ}\mathrm{C}$.

tangency of the curves is more and more different when increasing the prestrain is not so obvious as at 23 °C. This difference of behavior is certainly due to the fact that the loss peak is reached in between these two temperatures and that the slope of the loss factor changes and certainly creates unstability (cf. Fig. 18).

This is clearly a limitation of the way the rig has been conceived. The (Ox) rocking mode has indeed been translated in the frequency range of interest (from 400 to 1400 Hz, Section 2.3) in presence of the prestress beam.

The conclusion is that the frequency–prestrain superposition hypothesis is not verified. The loaded damping designs do not damp as expected: the low and high parts of each data do not superimpose, consequently the loss factor does not collapse into one single curve. Examination of the figures rather suggests that a second translation along the vertical axe should be required to collapse the data. Off the (Ox) rocking mode that could be erased, prestrain is certainly accompanied by many nonlinear phenomenons that cannot be quantified and explained at this stage.

Fig. 21 however illustrates that a given master curve may not do so bad a job at interpolating behavior for various prestrains. It suggests that the prestrain curves could be used in physical frequencies to predict the material response to a dynamic load in presence of press forming.

4. Conclusion

A dynamic test rig has been designed and built to measure directly the complex shear stiffness of homogeneous viscoelastic films in steel–polymer–steel sandwich plates. The novelty of this test system is its ability to induce static prestrain in the viscoelastic layer.

The additional elements needed to insert the prestress beam lead to a resonant rig that has been characterized through a FE analysis. The main resonances observed in the experimental measured FRFs have been identified through the FE computation. The FE rig analysis has shown the rig to be capable of studying a large variety of sandwich plates with a thin viscoelastic core (close to the geometrical characteristics of the treated sample) over the range 1–2000 Hz. The rig allows us to characterize accurately damping films with a shear modulus up to 10^8 Pa, whatever the loss factor.

Results for a particular sample in the frequency range 1–2000 Hz, prestrain 0–3, at temperatures 0–50 °C have been shown. After smoothing and undersampling the measured data obtained at various temperatures, the frequency–temperature superposition hypothesis has been investigated and used to get a temperature-reduced frequency master curve. This representation leads to a non-parametric description of the complex

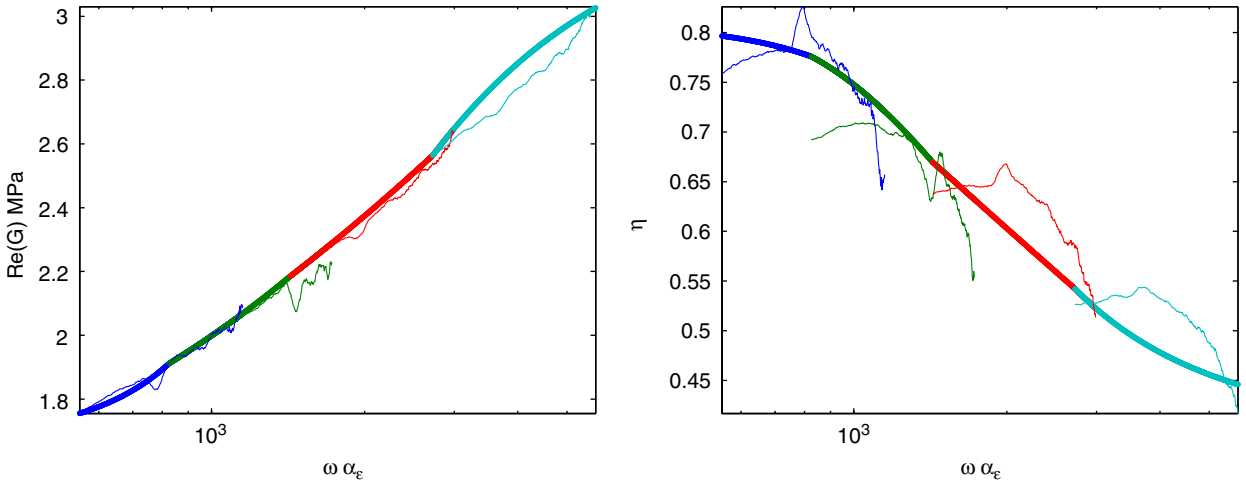

Fig. 21. Undersampled master curve against prestrain-reduced frequency $\omega\alpha_{\varepsilon_0}$ (cf. Eq. (7)). $\varepsilon_0 \in [0, 0.32, 1.33, 2.22]$, $T = 35\,^{\circ}\mathrm{C}$.

modulus that can be used in FE modeling, in order to predict the dynamic behavior of damped structures incorporating such viscoelastic films.

The effect of prestress on the damping of this material has been investigated by using the same methodology with various prestrains. It has shown that the frequency–prestrain superposition hypothesis is not applicable to the measurements, since the loss factor does not collapse into one single curve. The expected behavior described by many authors (increasing of the modulus and decreasing of the loss factor with prestrain) has been observed, but the measurements indicate that the loaded damping designs do not damp as expected. However, the influence of the prestrain on the complex shear modulus has been quantified for a particular viscoelastic film. The results provide frequency–prestrain constitutive laws for use in FE models of sandwich plates, particularly when the sandwich plate is press formed.

References

[1] P. Plunkett, C. Lee, Length optimization for constrained viscoelastic layer damping, *JASA* 48 (1) (1970) 150–161.
[2] A. Nashif, D. Jones, J. Henderson, *Vibration Damping*, Wiley, New York, 1985.
[3] M.D. Rao, Recent applications of viscoelastic damping for noise control in automobiles and commercial airplanes, *India–USA Symposium on Emerging Trends in Vibration and Noise Engineering*, 2001.
[4] E. Balmès, S. Germès, Design strategies for viscoelastic damping treatment applied to automotive components, *International Modal Analysis Conference*, Dearborn, 2004.
[5] E. Balmès, Incorporating damping predictions in the vibroacoustic design process, *International Seminar on Modal Analysis*, Leuven, 2004.
[6] ARCELOR, Fabricant d'acier, ⟨http://www.arcelor.com/⟩.
[7] H. Oberst, K. Frankenfeld, Über die Dämpfung der Biegeschwingungen dünner Bleche durch festhaftende Beläge, *Acustica* 2 (1952) 181–194.
[8] C. Van't Hof, P. Mohanty, D. Rixen, Testing a dynamic mechanical analyser: influence of the measuring column dynamics, *International Modal Analysis Conference*, 2003.
[9] N. Herrmann, *Application of Ultrasonic Techniques to the Study of Dispersions*, PhD Thesis, University of Louis Pasteur, Strasbourg, France, 1997.
[10] D. Ross, E. Ungar, E. Kerwin, Damping of plate flexural vibrations by means of viscoelastic laminates, in: J. Ruzicka (Ed.), *Structural Damping*, vol. 51, 1959.
[11] B. Allen, A direct complex stiffness test system for viscoelastic material properties, *Proceedings of Smart Structures and Materials*, San Diego, USA, February 1996.
[12] LMS CADA-X, *The System Solution for Integrated Test Laboratory*, Leuven Measurements & Systems, Leuven, Belgium, 1990.
[13] E. Balmès, J. Leclère, *Structural Dynamics Toolbox 5.0 (for use with MATLAB)*, SDTools, Paris, France, ⟨http://www.sdtools.com⟩, July 2002.

[14] G. Kergourlay, E. Balmès, D. Clouteau, Interface model reduction for efficient fem/bem coupling, *International Seminar on Modal Analysis*, Leuven, September 2000.
[15] J. Biggerstaff, J. Kosmatka, Shear measurements of viscoelastic damping materials embedded in composite plates, *Proceedings of SPIE Symposium on Smart Structures and Materials*, 1999.
[16] J. Salençon, *Viscoélasticité, Presse des Ponts et Chaussés*, Paris, 1983.
[17] J. Halary, *Traitement pratique des résultats des essais de viscoélasticité p169–189 in Introduction à la mécanique des polymères*, Inpl-Mecamat-Gfp-Apollor-Firtech-Christian G'Sell-Jean-Marc Haudin, 1998.
[18] M. Williams, R. Landel, J. Ferry, The temperature dependance of relaxation mechanisms in amorphous polymers and other glass forming liquids, *Journal of American Chemical Society* 77 (1955) 3701–3707.
[19] G. Kergourlay, *Mesure et Prédiction de Structures Viscoélastiques—Application à une Enceinte Acoustique*, PhD Thesis, Ecole Centrale de Paris, 2004.